Supplement of Atmos. Chem. Phys., 25, 6943–6955, 2025
https://doi.org/10.5194/acp-25-6943-2025-supplement

Supplement of

Measurement report: Crustal materials play an increasing role in elevating particle pH – insights from 12-year records in a typical inland city of China

Hongyu Zhang et al.

Correspondence to: Shenbo Wang (shbwang@zzu.edu.cn) and Zhangsen Dong (dzszzu1990@163.com)

Text S1 Instruments and Measurements.

Samples were collected using a high-volume sampler (TE-6070D, Tisch, USA) and air particulate samplers (TH-16A, Tianhong, China) from April 2011 to December 2022. Two quartz filters and two Teflon filters were used daily from 10:00 AM to 9:00 AM the next day, resulting in a total of 5848 samples. After excluding abnormal data due to instrument malfunctions, 4228 valid samples were obtained. Detailed information on the samples is provided in Table S1.

Organic carbon (OC) and elemental carbon (EC) were analyzed using a carbon analyzer (Model 5L, Sunset Laboratory, USA). The analysis of EC and OC was conducted in two stages. In the first stage, the filter membrane was placed in a quartz heating furnace under a pure helium atmosphere. As the temperature gradually increased to approximately 580°C, OC was volatilized and released. In the second stage, heating continued in a mixed atmosphere of 2% oxygen and 98% helium. When the temperature reached approximately 870°C, EC underwent oxidative decomposition and was released. During the helium flow transmission, OC and EC released at different temperatures were completely oxidized to CO_2 in a MnO_2 oxidation furnace and subsequently reduced to CH_4 for detection by a flame ionization detector (FID). The detection limits for both OC and EC were 0.2 μg/cm^2. Before each sample analysis, calibration was performed using a standard sucrose solution. Additionally, parallel tests were conducted every ten samples to ensure accuracy.

Water-soluble inorganic ions (Cl^-, NO_3^-, SO_4^{2-}, Na^+, NH_4^+, K^+, Mg^{2+}, and Ca^{2+}) were measured using ion chromatography (ICS-90 and ICS-900 models, Dionex, USA). Half of the $PM_{2.5}$ filter was cut into pieces and ultrasonically extracted with 20 mL of Milli-Q water for 30 min, followed by filtering through a 0.45 mm polytetrafluoroethylene syringe filter before analysis. The cation concentrations were determined by an IonPacASll-HC4 mm anion separation column and an

IonPacAGll-HC4 mm guard column, with 20 mM methane sulfonate as an eluent at 0.8 mL/min. The anions were measured by an IonPacCS12A cation separation column and an IonPacCG12A guard column, with a solution of 8.0 mM Na_2CO_3 + 1.0 mM $NaHCO_3$ as an eluent at 1.0 mL/min. The regression coefficients (R^2) of the calibration curves were over 0.9996 for all ions, except NH_4^+ (0.9988), which showed a quadratic response.

Elements were analyzed using a wavelength dispersive X-ray fluorescence spectrometer (S8 TIGER, Bruker, Germany) to determine concentrations of Fe, Na, Mg, Al, Si, Cl, K, Ca, V, Ni, Cu, Zn, Cr, Mn, Co, Cd, Ga, As, Se, Sr, Sn, Sb, Ba, and Pb (Tremper et al., 2018), which has been approved by the United States Environmental Protection Agency (Chow and Watson, 1994). The spectrometer was equipped with an X-ray tube featuring close coupling among the tube, sample, and detector, ensuring high efficiency and optimal excitation of elements within the sample. Before analysis, the instrument was calibrated using a series of high-quality, self-prepared standards. Calibration procedures were conducted following established methods (Chow and Watson, 1994). To assess potential contamination and ensure data quality, blank filters were routinely analyzed alongside each batch of samples.

Figures

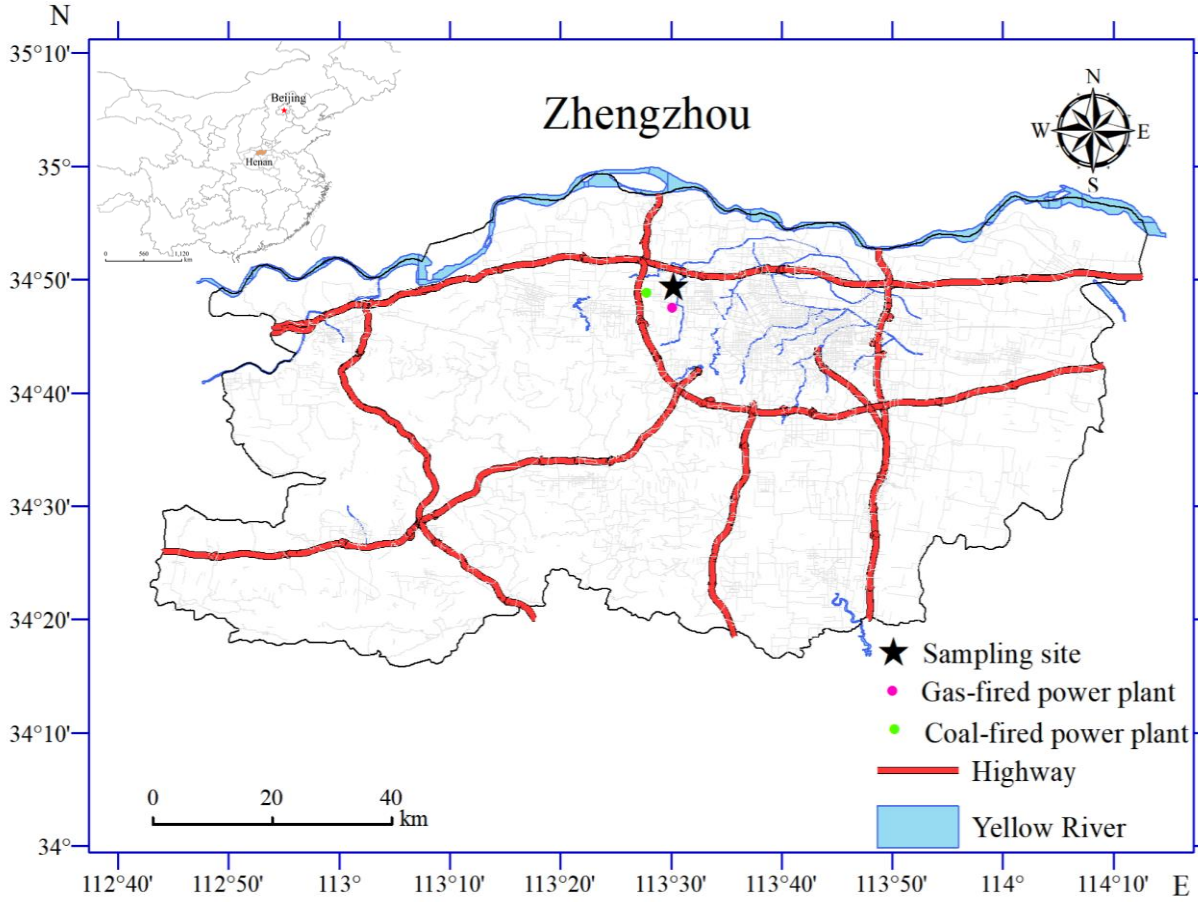

Figure S1. Sampling site in Zhengzhou, China.

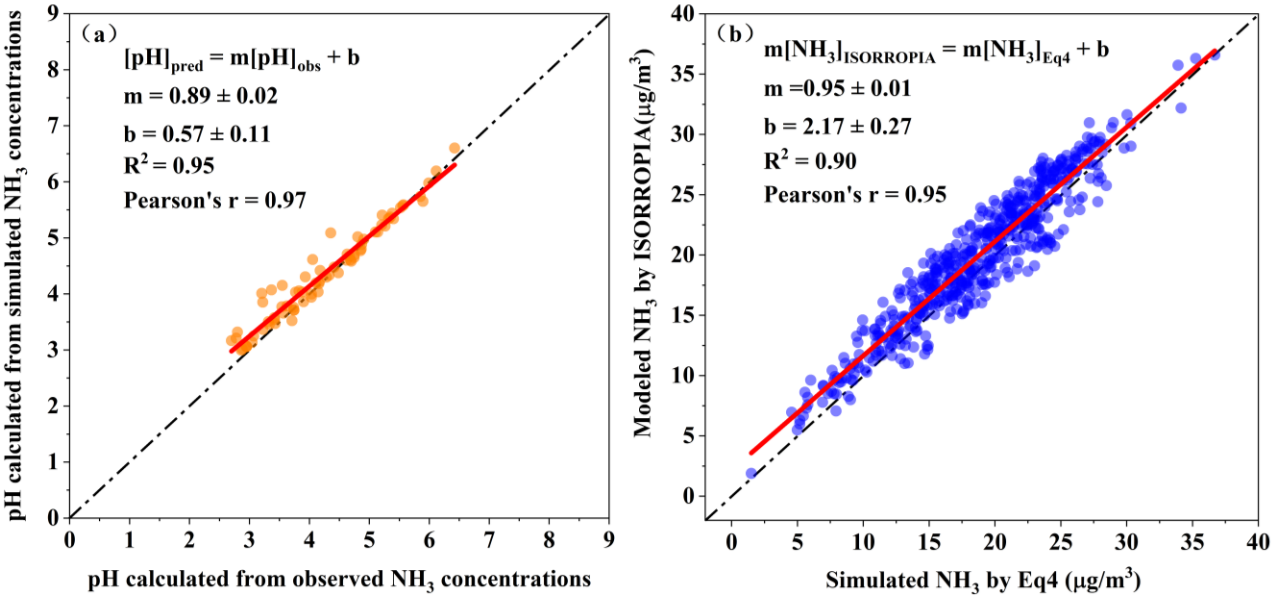

Figure S2. (a) Validation of pH estimates derived from observed vs. simulated NH_3 concentrations in 2022. Red line: linear regression fit. (b) Cross-validation of NH_3 concentrations calculated by the ISORROPIA thermodynamic model and Equation 4 (2011–2022). Red line: linear regression fit.

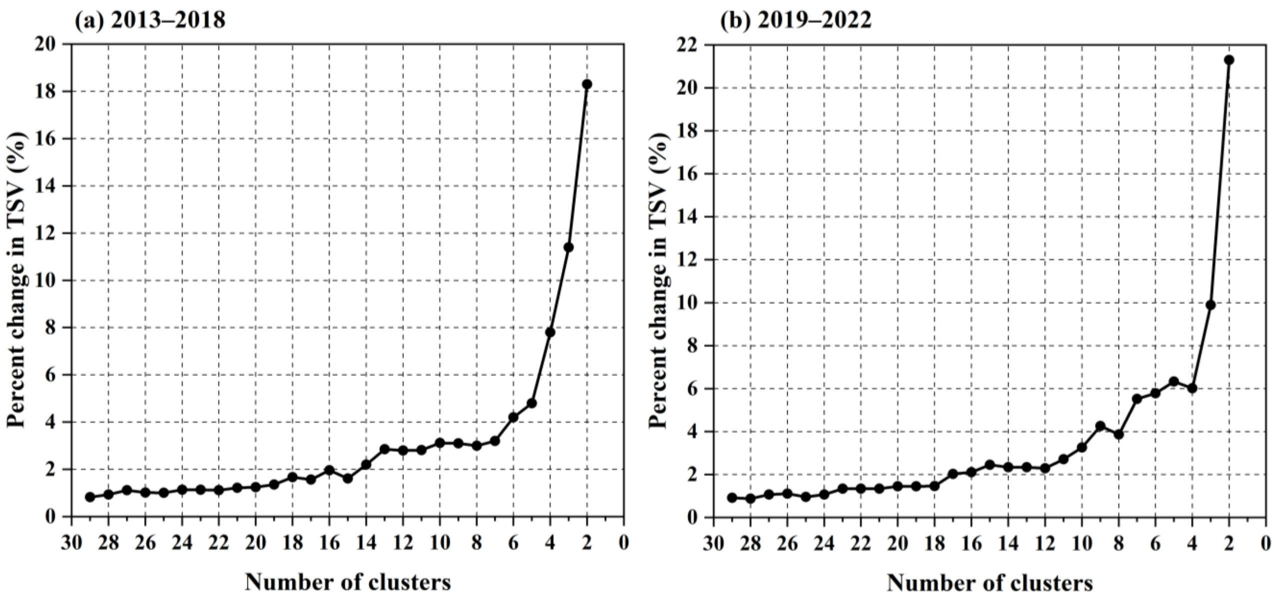

Figure S3. Evolution of total spatial variance (TSV) and optimal cluster number determination for backward trajectories under two policy phases: (a) 2013–2018; (b) 2019–2022

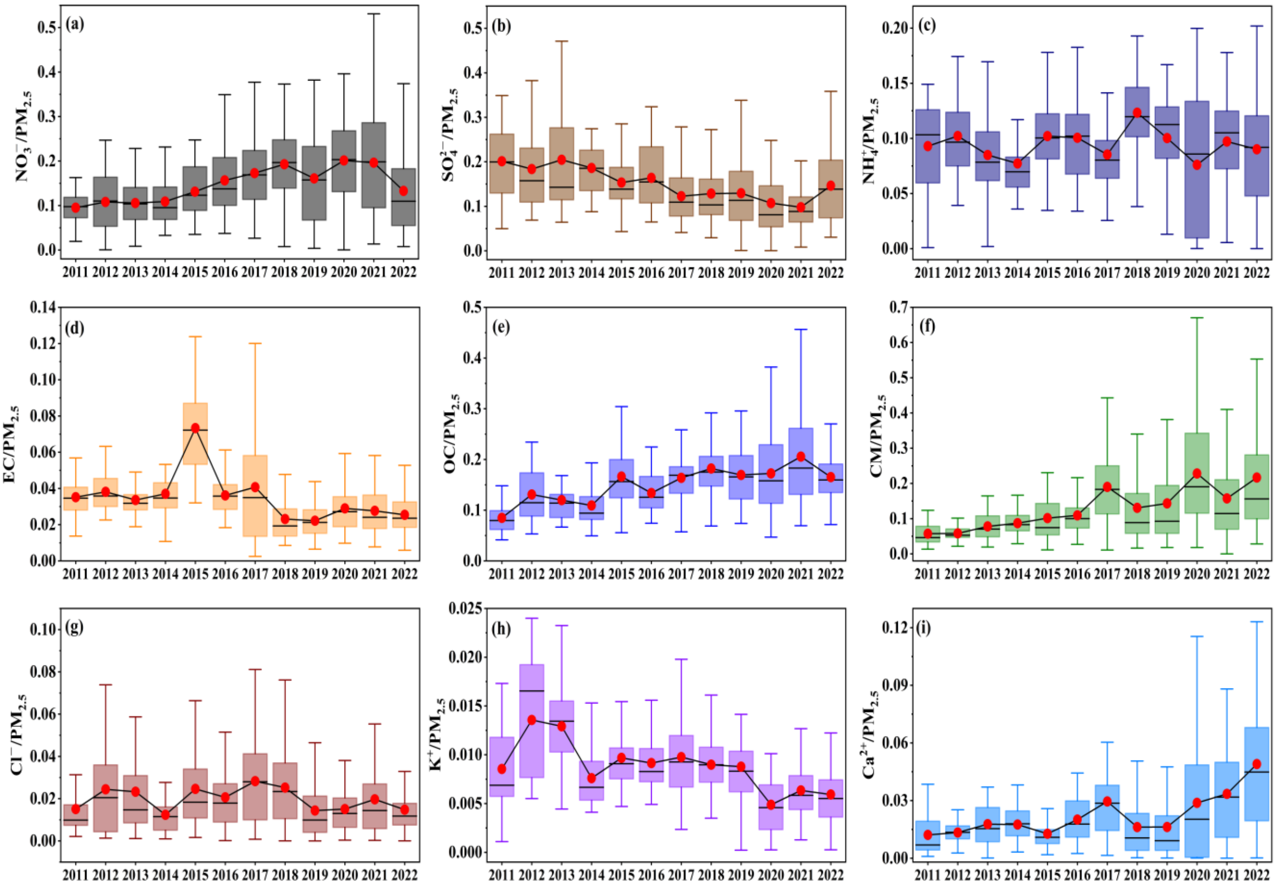

Figure S4. Trends in the proportions of chemical components in $PM_{2.5}$ from 2011 to 2022.

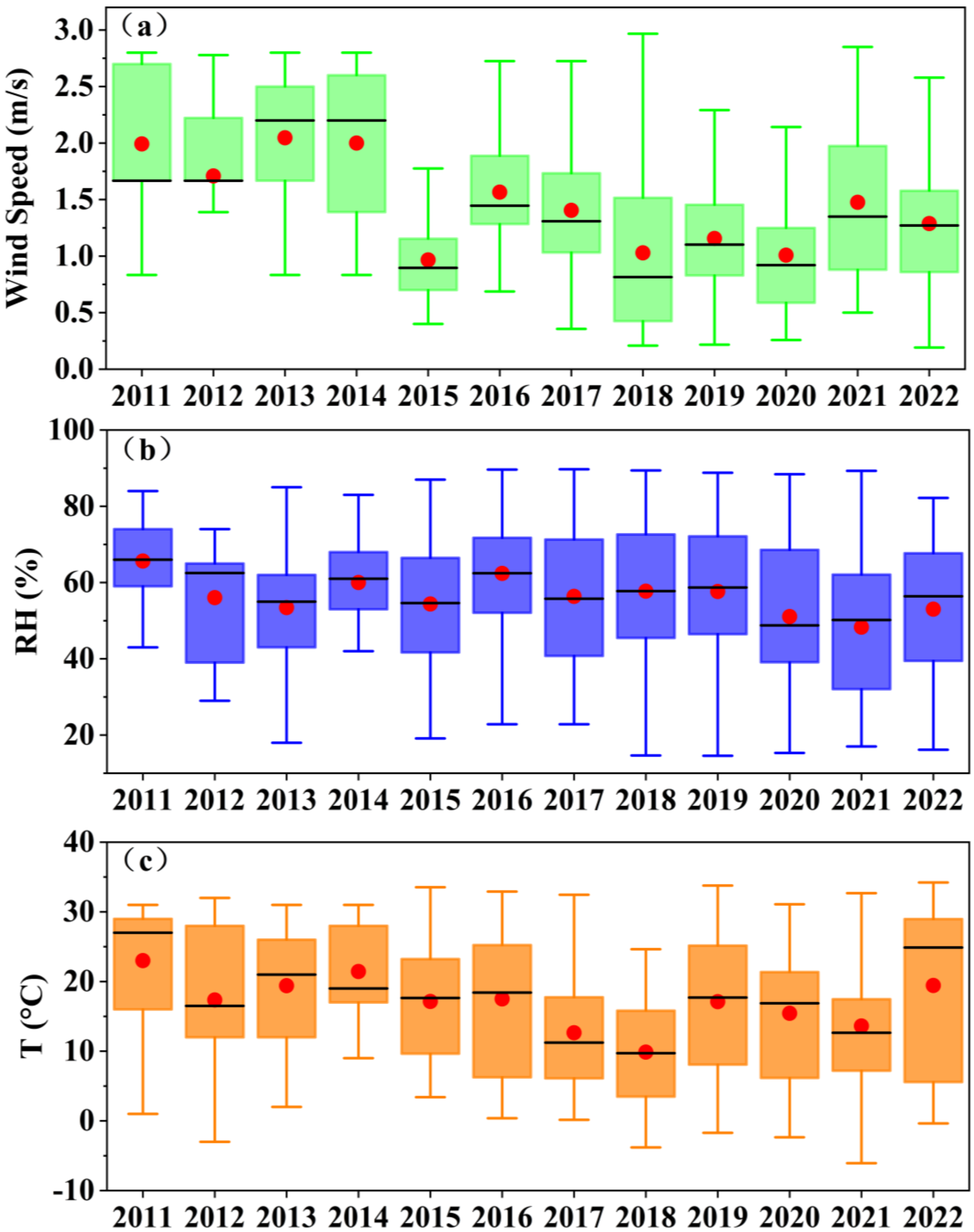

Figure S5. Trends in the meteorological parameters from 2011 to 2022.

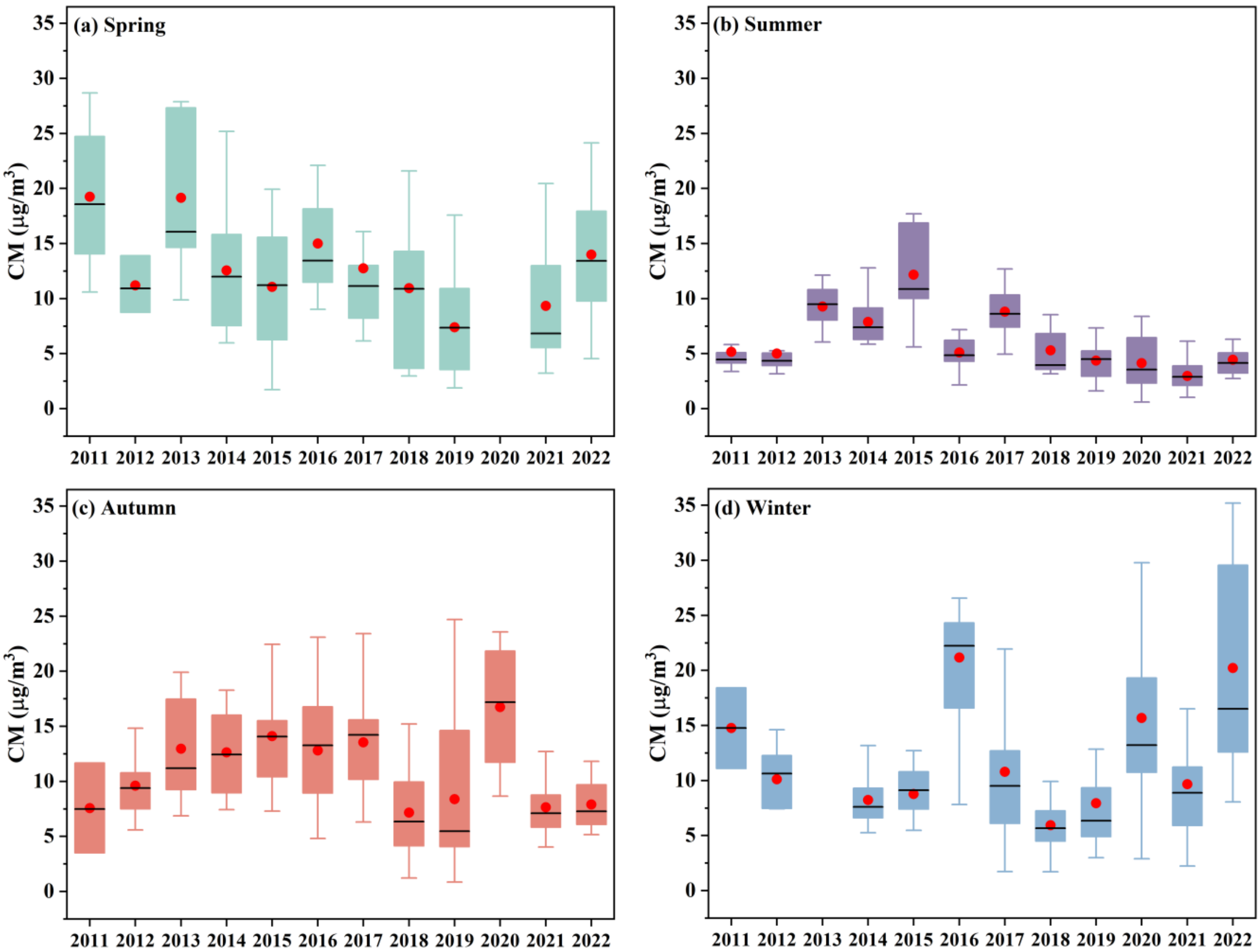

Figure S6. Trends in the CM concentrations in different seasons from 2011 to 2022.

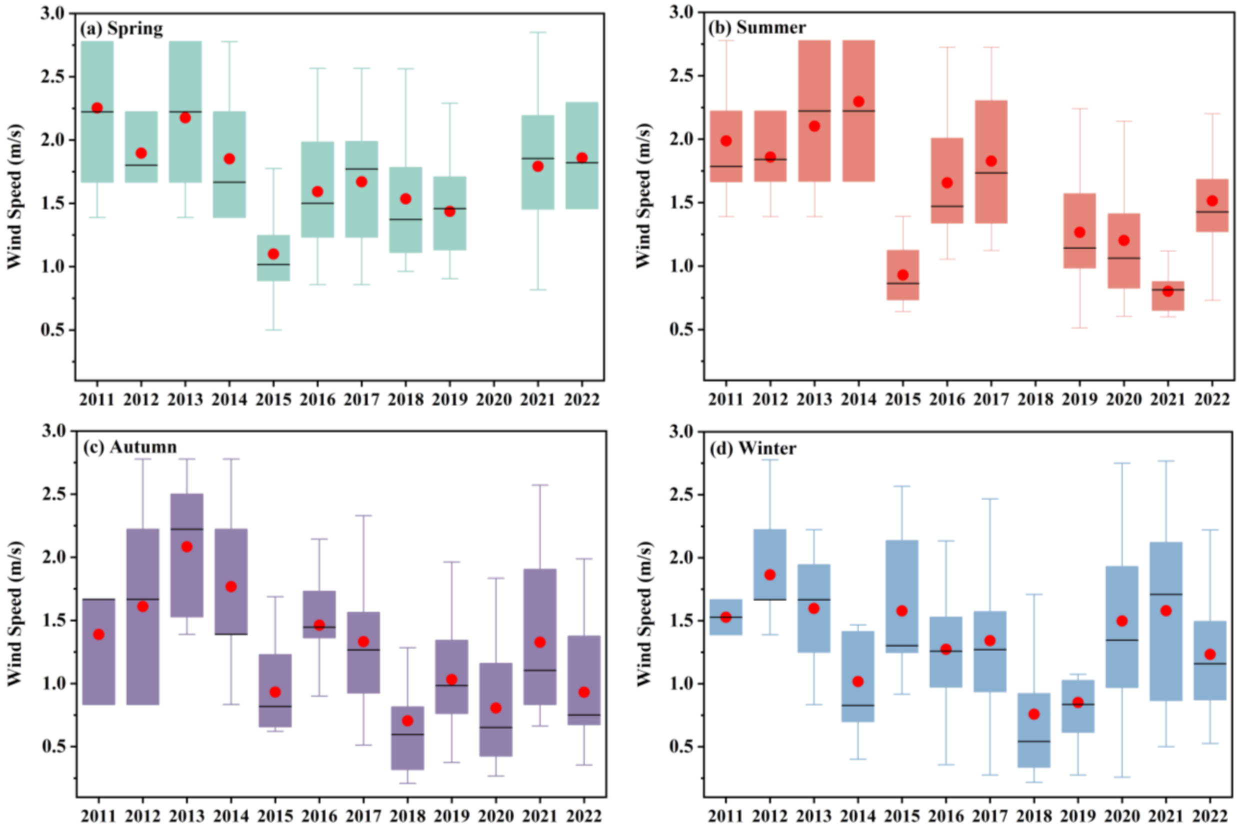

Figure S7. The variation in WS across different seasons from 2011 to 2022.

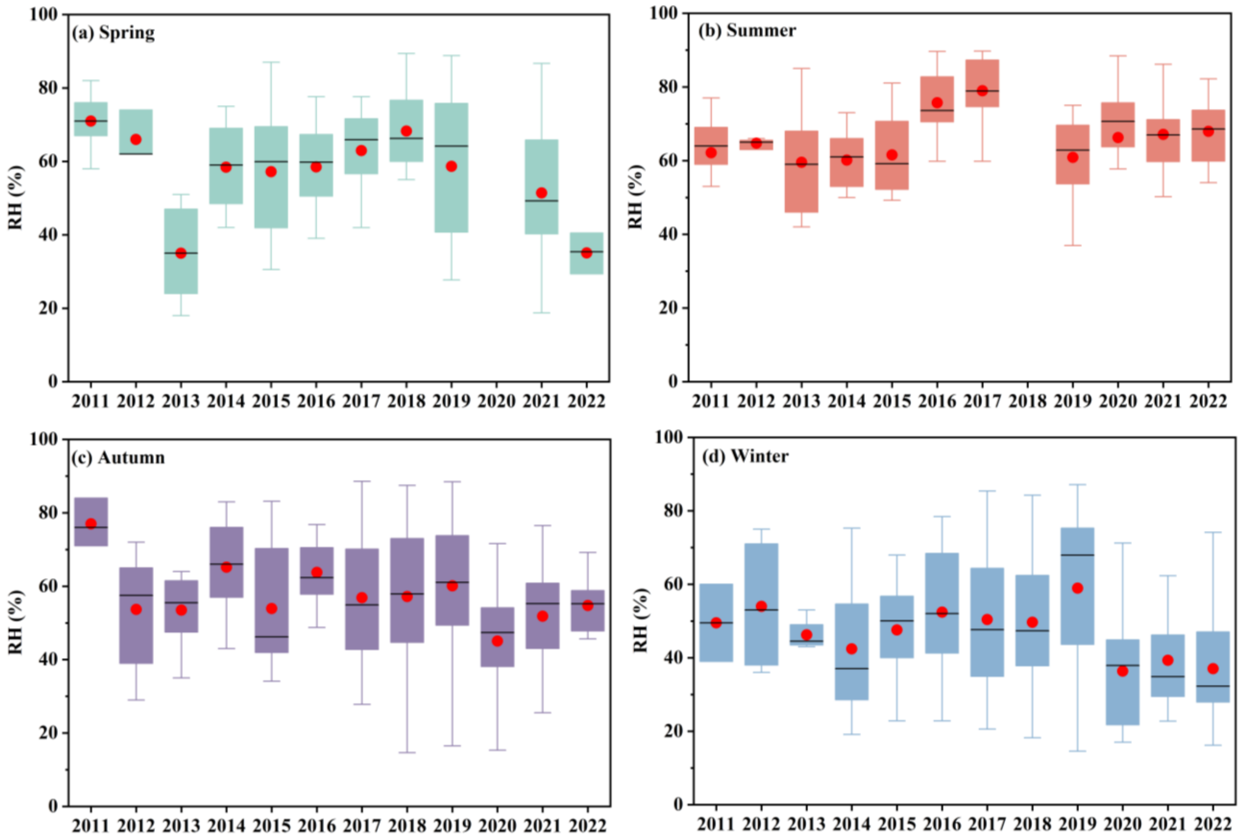

Figure S8. The variation in RH across different seasons from 2011 to 2022.

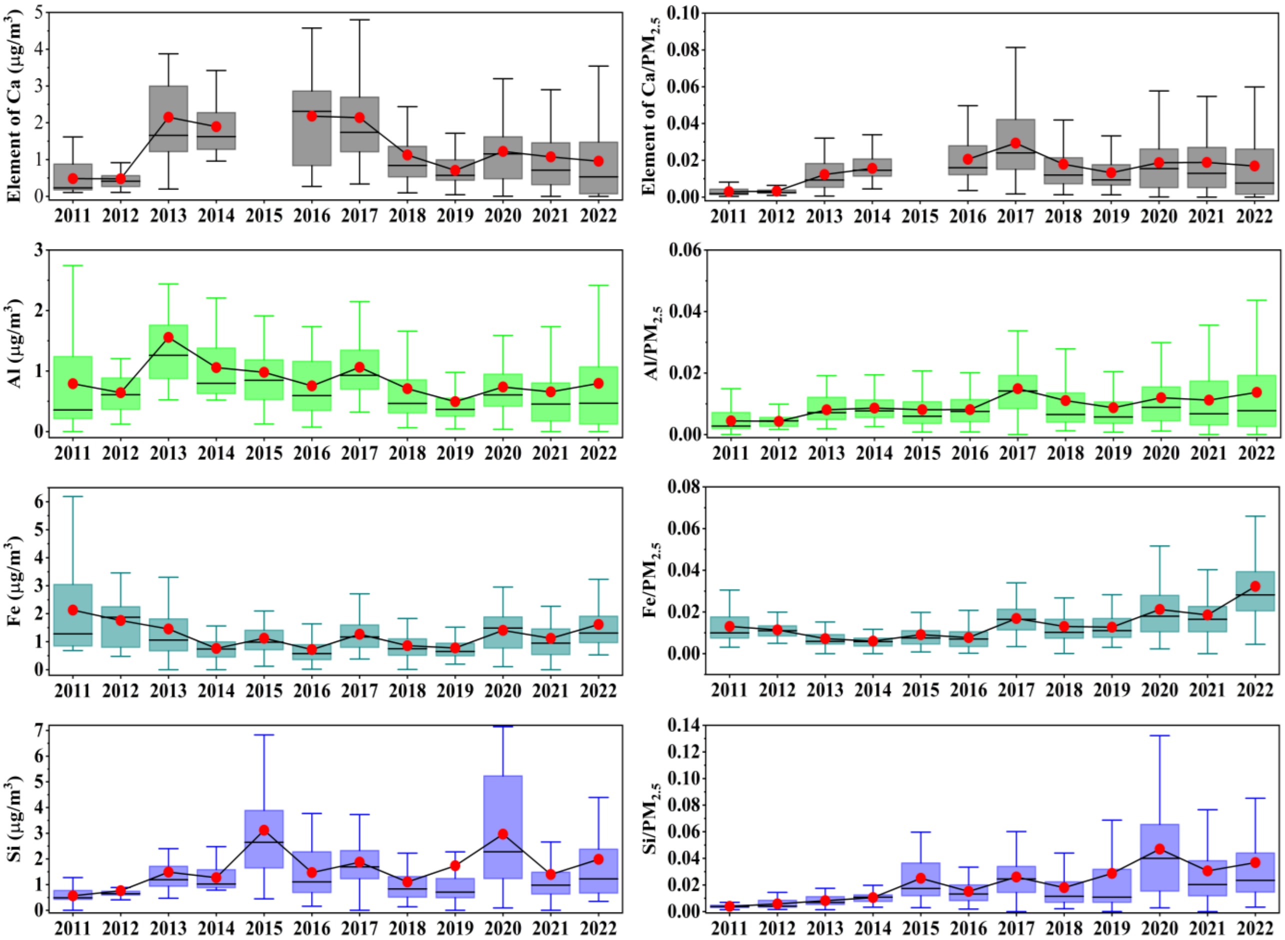

81
82 Figure S9. Trends in the concentrations of crustal elements and their proportions in $PM_{2.5}$ from 2011
83 to 2022.
84

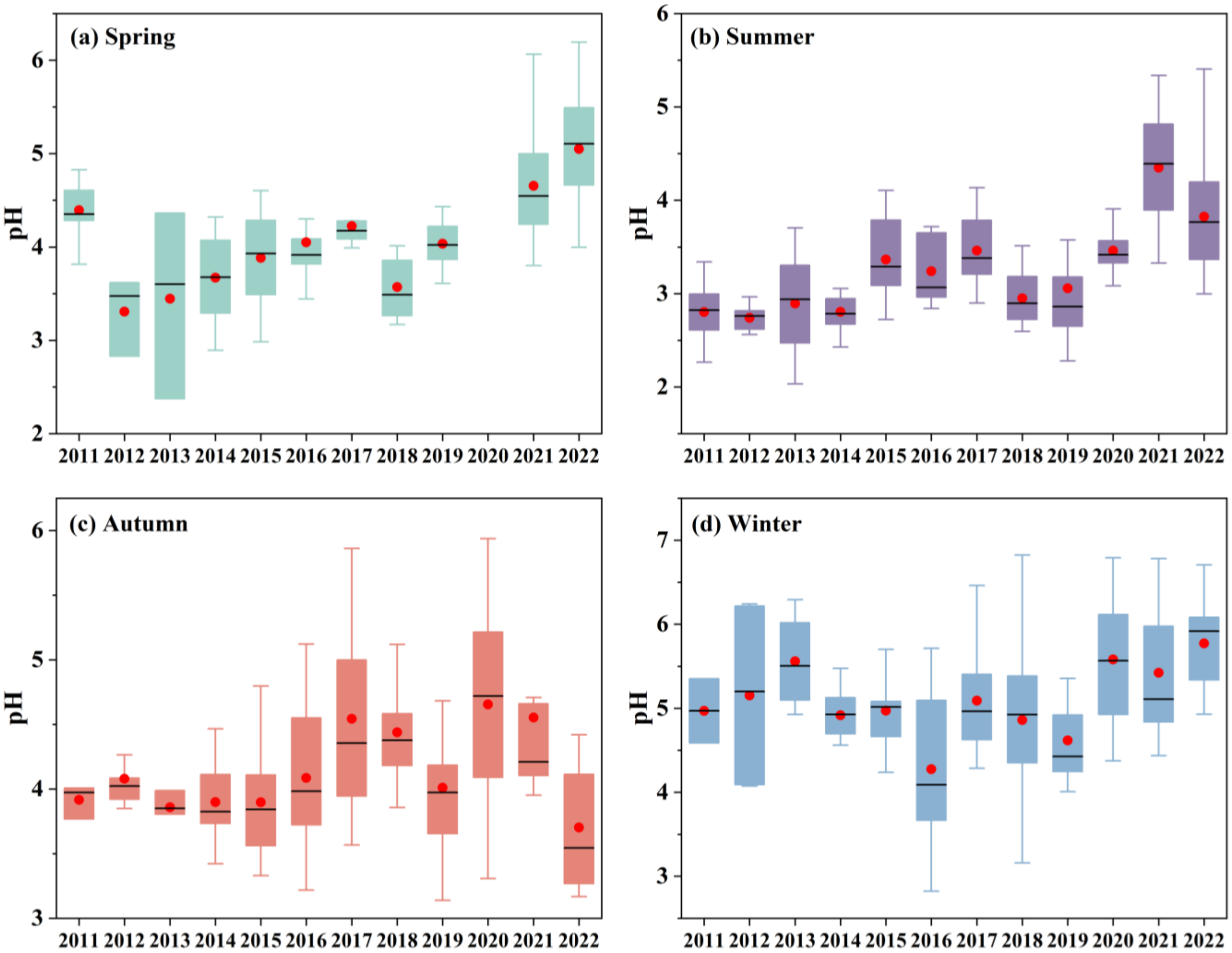

Figure S10. Trends in the particle pH in different seasons from 2011 to 2022.

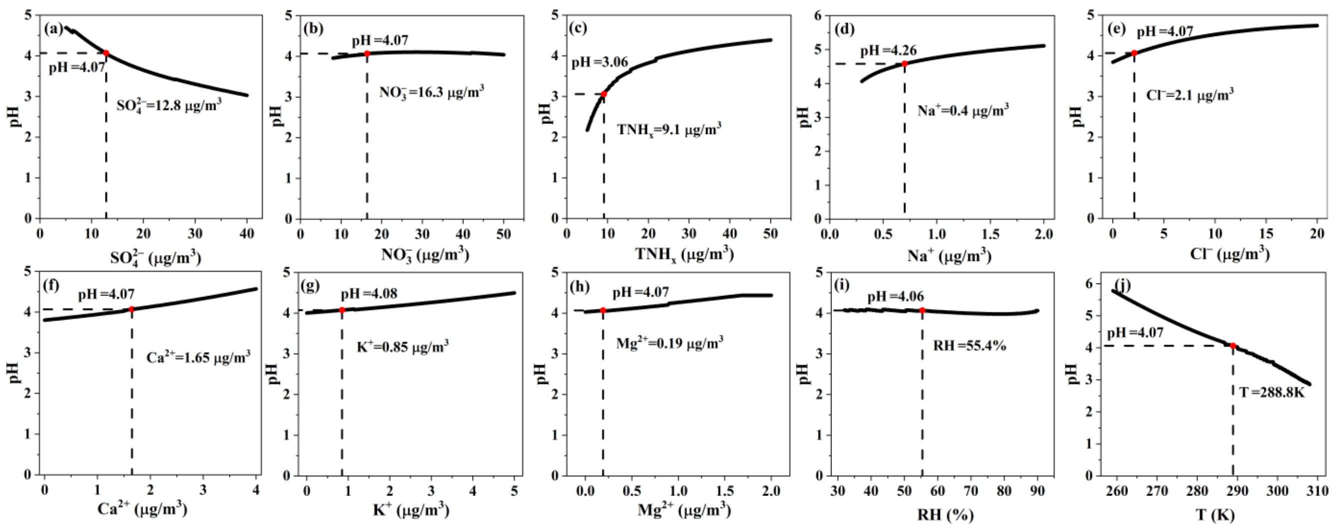

Figure S11. Sensitivity analysis of input parameters to particle pH. The dashed line represents the average of the observational data from 2011 to 2022.

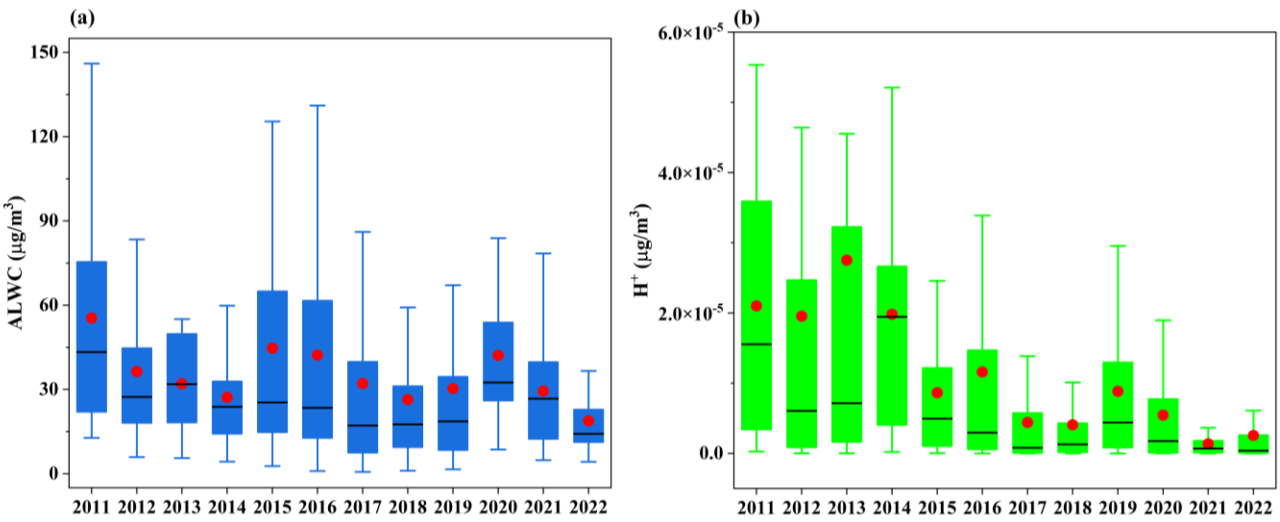

Figure S12. Trends in aerosol liquid water content (ALWC) and H^+ concentrations from 2011 to 2022

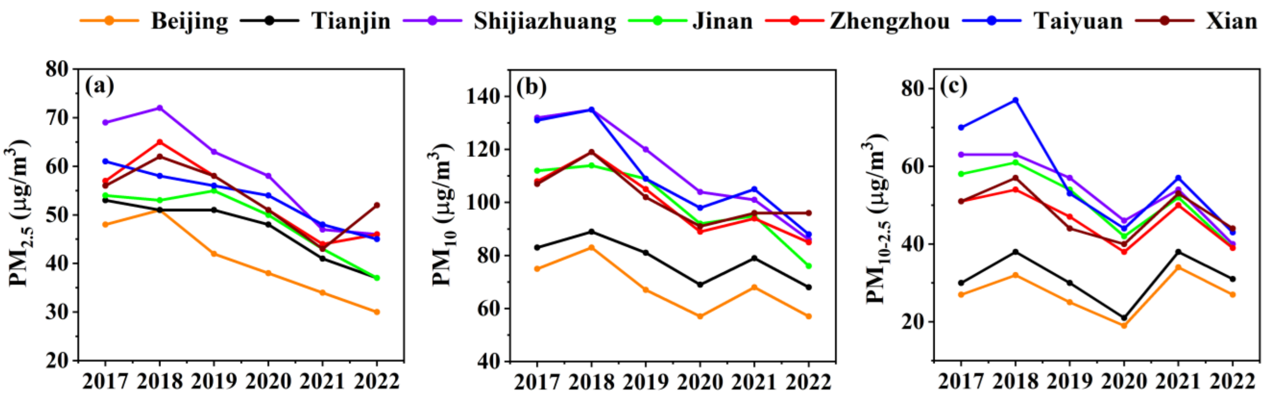

Figure S13. Trends in the annual average concentrations of $PM_{2.5}$, PM_{10}, and $PM_{10\text{-}2.5}$ in provincial capitals in the North China Plain.

Tables

Table S1. Information on sampling date and numbers.

Years	Sampling date	The effective number of samples
2011	April 7–20 July 1–31 October 28–December 2 December 11–November 23	188
2012	February 25–26 April 21–May 6 July 22–August 2 October 17–November 1 December 8–25	140
2013	February 25–March 6 April 1–May 1 June 5–July 30 September 20–October 13 December 2–18	184
2014	April 1–May 5 June 18–July 20 October 7–24 December 30–31	180
2015	January 1–15 April 1–20 July 1–20 October 9–24	248
2016	January 6–22 April 8–30 July 9–31 October 1–20 December 29–31	252
2017	January 1–20 April 18–May 4 July 1–26 October 14–December 31	480
2018	January 1–31 April 1–30 July 1–31 October 9–December 31	600
2019	January 1–31 April 1–30 July 1–31 September 2–October 31 November 12–30 December 21–31	592

2020	January 1–20 June 5–July 31 October 6–November 13 December 15–31	332
2021	January 1–31 March 16–April 30 July 1–August 8 October 17–December 31	540
2022	January 1–4 April 1–May 3 July 1–August 11 September 5–October 11 December 10–31	492
Total		4228

Table S2. The method detection limit (MDL) and measurement uncertainties (Unc) of individual components

	MDLs (μg/m^3)	Unc (%)
EC	0.1	13.1
OC	0.1	9.8
Na^+	0.005	9.6
NH_4^+	0.011	10.1
K^+	0.006	9.5
Mg^{2+}	0.002	9.3
Ca^{2+}	0.017	8.8
F^-	0.001	8.2
Cl^-	0.001	9.3
NO_3^-	0.015	10.1
SO_4^{2-}	0.031	9.9
Na	0.003	10.9
Mg	0.002	10.6
Al	0.004	9.2
Si	0.005	9.3
Cl	0.008	9.5
K	0.005	9.4
Ca	0.01	9.4
V	0.008	57.9
Ni	0.006	96.6
Cr	0.02	24.7
Mn	0.02	16.8
Fe	0.03	9.3
Co	0.009	79.6
Cu	0.005	5.8
Zn	0.003	8.4
Ga	0.005	84.7
As	0.008	27.4
Se	0.006	25.7
Sr	0.006	22.8
Cd	0.03	68.6
Sn	0.02	42.0
Sb	0.02	73.6
Ba	0.02	15.6
Pb	0.02	13.4

Table S3. Major emission reduction measures were implemented during the Air Pollution Prevention and Control Action Plan (2013–2018) and the Three-Year Action Plan (2018–2020)

	Air Pollution Prevention and Control Action Plan	Three-Year Action Plan
Industrial Restructuring	Elimination of a large amount of outdated production capacity in industries. Cement to optimize the industrial structure Reduce high-pollution production	Continued phase-out of outdated production capacity (e.g., steel, cement) Strengthen ultra-low emission retrofitting in sectors such as steel and coking
Energy Transition	Capping coal consumption in certain regions Restricting the construction of small-scale coal-fired power plants	Deepen regional coal consumption control Expand clean heating coverage in rural areas
Promote clean fuels in the residential sector	Ultra-low emission retrofitting in the power sector Comprehensive retrofitting of coal-fired boilers	Continue raising emission standards in the power sector Introduce ultra-low emission requirements for non-power sectors (e.g., steel, coking)
Mobile Source Control	Initial elimination of high-emission (yellow-label) vehicles Promotion of China V emission standards	Full implementation of China VI emission standards Set up low-emission zones for diesel trucks Promote the replacement of vehicles with new energy vehicles

Coordinated Control of Multiple Pollutants	Focus on SO_2, NO_x, and $PM_{2.5}$	Incorporate VOCs (Volatile Organic Compounds) and NH_3 (ammonia) into joint control Strengthen control over industrial solvent use and agricultural emissions
Innovative Governance Models	Regional joint prevention and control (key regions such as Beijing–Tianjin–Hebei)	Grid-based and precise supervision (micro-zoning and dynamic management)

Table S4. The Comparison of Key Indicators Between the Air Pollution Prevention and Control Action Plan (2013–2018) and the Three-Year Action Plan (2018–2020).

	Air Pollution Prevention and Control Action Plan	Three-Year Action Plan
$PM_{2.5}$	Beijing-Tianjin-Hebei region: ≥25% reduction Yangtze River Delta region: ≥20% reduction Pearl River Delta region: ≥15% reduction	$PM_{2.5}$ concentrations to be reduced by more than 18% (vs. 2015)
PM_{10}	National PM_{10} concentration to decrease by ≥10%	No explicit targets
SO_2/NO_x	No explicit targets	National SO_2 and NO_x emissions to be reduced by ≥15% (vs. 2015)
Number of good air quality days	"Annual improvement" in good air days	>80% annually in prefecture-level and above cities
Number of heavily polluted days	No explicit targets	25% reduction in heavy pollution days (vs. 2015)

Table S5. Control measures for dust implemented by Henan Province and Zhengzhou government

Release time	Policies	Regulatory focus
2013.9	Regulations on Reducing Pollutant Emissions in Henan Province	Road, Construction
2014.8	Temporary Regulations on Dust Control Management at Construction Sites in Henan Province	Construction
2016.7	Implementation Plan for Controlling Dust Pollution in Henan Province	Road, Construction
2018.2	Regulations on the Prevention and Control of Atmospheric Pollution in Henan Province	Road, Construction, Piles
2019.4	Special Action Plan for Fine Management of Dust Pollution Prevention and Control at Construction Sites in Zhengzhou City, 2019	Construction
2019.8	Enhanced Action Plan for Intensive Dust Control at Construction Sites in 2019	Construction
2021.1	Special Governance Plan for Key Project Dust Pollution in Zhengzhou	Road, Construction, Piles

Table S6. Analysis of the inter - annual trends of CM and Ca^{2+} concentrations and pH during different periods using multiple methods.

	2011–2013			2013–2019			2019–2022		
	CM	Ca^{2+}	pH	CM	Ca^{2+}	pH	CM	Ca^{2+}	pH
MK-*Z*	3.01	2.70	1.41	–9.74	–13.62	3.00	2.48	8.21	5.12
MK-*p*	0.003	0.007	0.159	<2.2 E–16	<2.2E–16	0.003	0.013	2.20E–16	2.99E–07
Sen's slope	0.082	0.023	7.10E–03	–0.015	–4.14E–03	9.15E–04	5.80E–03	5.42E–03	2.93E–03
LS slope	2.65	0.61	/	–0.81	–0.32	0.11	0.24	0.40	0.21

** MK-*Z* and MK-*p* represent the trend (Z) and significance (*p*) calculated by the Mann - Kendall method respectively; Sen's slope represents the Sen slope; LS slope represents the Least - Squares slope. All the above calculations were performed using the R language (R version 4.0.2).

Table S7. The ratios of Ca/Si in the source spectrum of different dust sources in China

Dust source	City	Ca/Si	Reference
Road dust	Xi’an	2.04	http://www.klacp.ac.cn/wgPMzypfypk/ycy/201706/t20170610_375562.html
	Yinchuan	2.48	
	Lanzhou	1.67	
	Beijing	1.25	
	Tianjin	1.03	
	Baoding	1.16	
	Shijiazhuang	1.98	
	Handan	1.83	
	Shenyang	1.81	
	Changsha	1.92	
	Chongqing	1.38	
	Chengdu	1.17	
	Kunming	1.94	
	Taiyuan	1.55	
	Nanjing	1.28	
Construction dust	Xi’an	1.69	http://www.klacp.ac.cn/wgPMzypfypk/ycy/201706/t20170610_375562.html
	Yinchuan	1.84	
	Lanzhou	2.33	
	Beijing	2.65	
	Tianjin	1.46	
	Baoding	1.58	
	Shijiazhuang	1.38	
	Handan	1.86	
	Shenyang	1.92	
	Changsha	2.30	
	Chongqing	2.52	
	Chengdu	2.15	
	Kunming	1.60	
	Taiyuan	1.92	
	Nanjing	2.26	
Piles dust	Xi’an	0.72	(Yang, 2016)
	Tianjin	0.57	(Zhang et al., 2018)
	Taiyuan	0.61	(Bi et al., 2007)
	Jinan	1.01	(Bi et al., 2007)
	/	0.65	http://www.nkspap.com:9091/Index.aspx
Soil dust	Nanchang	0.37	(Xu et al., 2019)
	Xi’an	0.27	(Yang, 2016)
	Jincheng	0.13	(Wang et al., 2016)
	Wuhan	0.52	(Gong and Luo, 2018)
	/	0.53	http://www.nkspap.com:9091/Index.aspx

Table S8. The difference between component concentrations (μg/m^3) and meteorological parameters between adjacent years.

Years	ALWC	$H^+(10^{-6})$	NO_3^-	SO_4^{2-}	TNH_x	Na^+	Cl^-	K^+	Ca^{2+}	Mg^{2+}	RH(%)	T (℃)
2012VS2011	−19.0	-1.5	4.0	−4.6	1.3	0.02	2.0	0.9	−0.2	0.04	−9.6	−5.7
2013VS2012	−4.6	-7.6	2.6	13.0	2.1	0.2	0.4	0.3	1.4	0.1	−2.6	2.1
2014VS2013	−4.5	7.9	−7.3	−14.6	−6.9	−0.4	−3.4	−1.6	−1.1	−0.2	6.6	2.0
2015VS2014	17.6	-11.2	5.2	−1.8	5.5	0.1	2.1	0.4	−0.6	0.6	−5.6	−4.2
2016VS2015	−2.3	3.0	−0.2	−4.5	−3.7	−0.03	−0.1	−0.4	0.5	−0.7	8.0	0.3
2017VS2016	−10.0	-7.2	−2.9	−5.3	−3.6	−0.2	−0.3	−0.2	−0.1	0.1	−6.0	−4.9
2018VS2017	−5.8	-0.3	−0.8	−2.4	1.3	−0.1	−0.8	−0.2	−0.1	−0.1	1.4	−2.8
2019VS2018	4.1	4.8	−3.0	−0.8	−2.2	−0.04	−0.7	−0.03	−0.1	−0.01	−0.1	7.3
2020VS2019	11.6	-3.4	4.9	−0.3	−0.9	0.1	0.1	−0.2	0.7	0.02	−6.6	−2.1
2021VS2020	−12.7	-1.5	−3.6	−2.3	0.2	−0.01	0.03	0.01	0.1	0.04	−2.8	−1.5
2022VS2021	−10.6	-1.5	−5.1	1.9	−1.4	0.03	−0.3	0.01	0.5	0.04	4.7	5.8

References

Bi, X., Feng, Y., Wu, J., Wang, Y., and Zhu, T.: Source apportionment of PM_{10} in six cities of northern China, Atmospheric Environment., 41, 903–912, https://doi.org/10.1016/j.atmosenv.2006.09.033, 2007.

Chow, J.C., Watson, J.G., 1994. Guidelines for PM_{10} sampling and analysis applicable to receptor modeling. Washington, DC7 US Environmental Protection Agency, Office of Air Quality Planning and Standards, EPA-452/R-94-009.

Gong, P. and Luo, Y.: Study on the characteristics of source profiles in Wuhan, Journal of Nanjing University of Information Science & Technology., 10, 579–589, https://doi.org/10.13878/j.cnki.jnuist.2018.05.008， 2018.

Tremper, A.; Font, A.; Priestman, M.; Hamad, S.; Chung, T.; Pribadi, A.; Brown, R.; Goddard, S.; Grassineau, N.; Petterson, K.; Kelly, F.; Green, D.: Field and laboratory evaluation of a high time resolution x-ray fluorescence instrument for determining the elemental composition of ambient aerosols, Atmos. Meas. Tech., 11, 3541–3557, https://doi.org/10.5194/amt-11-3541-2018, 2018.

Wang, Y., Peng, L., Li, L., Wang, Y., Zhang, T., Liu, H., and Mu, L.: Chemical compositions and sources apportionment of re-suspended dust in Jincheng, Environmental Science., 37, 82–87, https://doi.org/10.13227/j.hjkx.2016.01.012, 2016.

Xu, Y., Gong, X., and Zhang, W.: Construction and characteristic analysis of $PM_{2.5}$ source profiles of typical emissions in Nanchang City, Chemical Engineer., 33, 41–43, https://doi.org/10.16247/j.cnki.23-1171/tq.20190841, 2019.

Yang, Y.: The Chemical Compositions and source apportionment of particulate matter of open sources in Xi'an, 42–43, https://doi.org/10.27393/d.cnki.gxazu.2016.000073, 2016.

Zhang, J., Wei, E., Wu, L., Fang, X., Li, F., Yang, Z., Wang, T., and Mao, H.: Elemental composition and health risk assessment of PM_{10} and $PM_{2.5}$ in the roadside microenvironment in Tianjin, China, Aerosol and Air Quality Research., 18, 1817–1827, https://doi.org/10.4209/aaqr.2017.10.0383, 2017.